Enhanced Faraday pattern stability with three-frequency driving

Yu Ding* and Paul Umbanhowar†
Department of Physics and Astronomy, Northwestern University, Evanston, Illinois 60208, USA
(Received 1 September 2005; revised manuscript received 3 March 2006; published 14 April 2006)

We report experimental observations of enhanced stability of quasipatterns and superlattice patterns in a vertically oscillated, deep viscous fluid layer with the addition of a third driving frequency. With two-frequency driving in the ratios 4:5 and 6:7, 12-fold quasipatterns and type-I superlattice patterns appear, respectively, as a secondary instability for a range of relative phases and amplitudes. Addition of a small third-frequency component at twice the difference frequency, i.e., 4:5:2 and 6:7:2, shifts the region of stability for these patterns closer to onset. For a range of parameter values the stabilized patterns become the primary instability. The degree of stabilization is sensitive to the amplitude and relative phase of the third-frequency term in qualitative agreement with a recent symmetry based analysis of resonant three-wave interactions.

DOI: 10.1103/PhysRevE.73.046305 PACS number(s): 47.54.−r, 89.75.Kd, 47.35.−i

INTRODUCTION

Pattern formation is common in nonlinear dissipative systems [1]. Examples of pattern forming systems include Rayleigh-Bénard convection [2], Taylor-Couette flow [3], vibrated granular materials [4], and reaction-diffusion systems [5]. Here we examine pattern formation in parametrically driven fluid surface waves, which were first studied by Faraday in 1831 [6]. When a fluid with a free surface is vertically oscillated, the initially flat surface loses stability beyond a critical acceleration amplitude, and surface waves form: patterns of stripes and squares are typically observed [7–10]. Faraday wave patterns provide a convenient experimental system for studying pattern formation because fast time scales and large aspect ratios are readily achieved. Also, since the wavelength is determined by the driving frequency, multiple characteristic length scales can be forced simultaneously via multifrequency driving. The driving function and the physical properties of the fluid (viscosity, surface tension, density, and depth) determine the pattern selection. Patterns near onset can be regarded as a superposition of plane waves, and the angles between the waves are determined by nonlinear interactions. Amplitude equations for the waves can be derived under the assumption of weak nonlinearity [11].

Single-frequency driving was used to accelerate the fluid in Faraday's original study [6] as well as in many subsequent investigations. Faraday waves driven with two frequencies were not investigated until the more recent work of Edwards and Fauve [12]. With two-frequency forcing, the amplitude and frequency ratios and the relative phase all play important roles in pattern selection in addition to the overall frequency and amplitude. Many new patterns are observed, for example, quasipatterns and superlattice patterns [12–15]. Müller found a set of parameters where patterns of hexagons and triangles were equally likely to appear when driven with two frequencies in the ratio 2:4 [16]. With the addition of a small amplitude third forcing frequency (2:4:1), the triangular patterns were preferentially stabilized. Also with three-frequency forcing, Arbell and Fineberg produced stable eightfold quasipatterns [15], and Epstein and Fineberg realized stabilization of a disordered state near the bicritical point and fast switching between hexagonal and superlattice patterns [17]. Recently, a series of patterns ("grid states") have been observed for which two hexagonal lattices are corotated such that the 12 critical wave numbers lie on a hexagonal sublattice [18].

Pattern selection in vertically oscillated fluid waves is typically described theoretically in terms of a resonant triad interaction in which two linearly unstable (critical) modes of equal wavelength quadratically couple via a third linearly stable (damped) mode which can be larger or smaller than the unstable mode. The wavelength of the damped mode determines the angle between the critical modes, which in turn selects the pattern. Silber and co-workers have shown that in parametrically forced, weakly damped systems, the strength of specific three-wave interactions can be determined for a damped mode of a given temporal response [19–21]. Using only symmetry considerations, the strength of the nonlinear resonant triad interaction is determined by the amplitude and relative phases of the individual driving frequencies [22]. In particular, with even:odd two-frequency driving where the even term is dominant, the damped mode mediated quadratic interaction is allowed, and can be enhanced with the addition of a third driving component with the proper frequency and phase.

Here we report experiments that systematically examine the changes in pattern selection which occur with the addition of a third driving frequency at twice the difference frequency of two different even mode dominant frequency ratios of 4:5 and 6:7.

I. EXPERIMENT

In our experiment a 0.65-cm-deep layer of 20 cS silicone oil is held in a cylindrical cell 7.0 cm in radius with a polyvinyl chloride sidewall, a 0.8-cm-thick glass bottom, and a plexiglass top covered with a thin, white plastic sheet which serves as a light diffuser. The cell is mounted on the ram of

*Electronic address: y-ding@northwestern.edu
†Electronic address: umbanhowar@northwestern.edu

a linear air bearing connected to an electrodynamic vibration exciter (shaker). An audio amplifier drives the shaker with a computer-generated wave form. Amplitudes and phases of the Fourier components of the acceleration, measured by an accelerometer, are used to tune the driving wave form. Fluctuations in the amplitudes of these components from their target values are less than 0.01%, while the total root-mean-square difference between the measured and target acceleration wave forms is less than 1%. To minimize variations in viscosity and surface tension, the fluid temperature is maintained at 25.3 ± 0.005 °C. Surface waves are visualized by projecting parallel light through the cell bottom. The fluid surface refracts the light, which then falls on the diffuser producing an image of the surface state [23]. A charge-coupled device camera mounted directly above the cell and synchronized with the driving is used to acquire 40 images uniformly distributed within the driving cycle.

For a frequency of 80 Hz, which is typical in our experiments, the wave number k of the pattern just above onset is 11.8 cm^{-1}. The corresponding dissipation length, defined as $l_d = 2\nu k/f$, is approximately 0.15 cm, where ν is the kinematic viscosity and f is the wave oscillation frequency. Since $kl_d \simeq 117$ and $kh \simeq 7.8$, our experiments are in the weakly dissipative and deep fluid layer limits [24].

The vertical acceleration of the cell is

$$a(t) = A_m \cos(m\omega t) + A_n \cos(n\omega t + \phi_n) + A_p \cos(p\omega t + \phi_p), \tag{1}$$

with $m:n=4:5$ or 6:7 and $p=2(n-m)$, and where ω is the base frequency. Note that we set $\phi_m = 0$ without loss of generality. The acceleration amplitudes A_i are measured in units of $g = 9.81\ \mathrm{m/s}^2$, where g is the acceleration due to gravity at the surface of the earth. We compare patterns for three-frequency driving with patterns for two-frequency driving, (i.e., $A_p = 0$) near the bicritical point for two-frequency driving with the A_m term ($m=4$ or 6) dominant. Thus, the pattern wave number is approximately equal to the wave number for single-frequency driving at $m\omega$. With 4:5 driving, there is a region in parameter space well above onset where 12-fold quasipatterns exist (see Fig. 1). With 6:7 driving, type-I superlattice patterns [13] are observed (see Fig. 2). We will demonstrate that by adding a small third-frequency component with the correct phase to the driving function, both quasipatterns and superlattice patterns appear near onset. By scanning the parameters A_i and ϕ_j ($i \in \{m,n,p\}, j \in \{n,p\}$), we will show that the stability of these patterns is strongly influenced by the third frequency driving term via A_p and ϕ_p.

We classify the experimental patterns by first computing the spatial Fourier power spectrum of the pattern image in polar coordinates $p(k,\alpha)$. The angular autocorrelation of energy on a circle with radius k at angle θ is

$$C_k(\theta) = \frac{\sum_\alpha P(k,\alpha) P(k,\alpha+\theta)}{\sum_\alpha P(k,\alpha) P(k,\alpha)}, \tag{2}$$

with $P(k,\alpha) = p(k,\alpha) - \langle p(k,\alpha) \rangle_\alpha$ as in earlier work [10,14]. $C_k(\theta)$ is evaluated at $k=k_m$, the magnitude of the primary pattern wave number. Hexagonal, superlattice, and 12-fold quasipatterns all have sixfold symmetry, so $C_{k_m}(60°)$ is nearly 1 for all three patterns. 12-fold quasipatterns have an additional maximum in C_{k_m} at $\theta = 30°$, while type-I superlattice patterns have a second maxima at $\theta = 22°$. For square patterns (including 2MS), $C_{k_m}(90°) \approx 1$. Accordingly, we use $C_{k_m}(60°)$, $C_{k_m}(22°)$, $C_{k_m}(30°)$, and $C_{k_m}(90°)$ to identify the patterns. Table I summarizes our classification scheme. Our results are not sensitive to the exact value of the threshold (0.6 here) since the transitions between different patterns are sharp. Finally, note that $C_{k_m}(\theta)$ depends on the phase in the cycle where an image is acquired and on the driving parameters; for a given set of parameters, the pattern state is determined using the image with the largest value of $C_{k_m}(\theta)$ for $\theta = \{22°, 30°, 60°, 90°\}$.

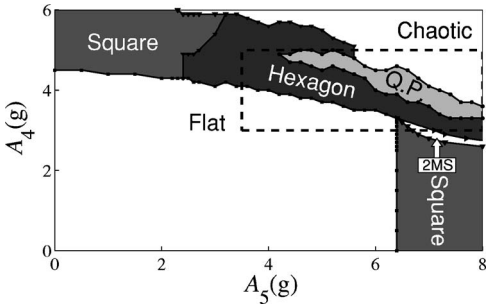

FIG. 1. Unperturbed phase diagram for 4:5 driving with $\omega/2\pi = 20$ Hz and $\phi_5 = 16°$. For hexagons and 12-fold quasipatterns (QP), the 4ω driving term is dominant (waves oscillate at 2ω), while for squares and square two-mode superlattice patterns (2MS) [14,15] the 5ω term is dominant. Dashed lines indicate the region where the higher acceleration resolution measurements of Fig. 3 are performed.

II. RESULTS

Figure 1 shows the fluid surface pattern states for 4:5 driving as a function of A_4 and A_5 at fixed relative phase.

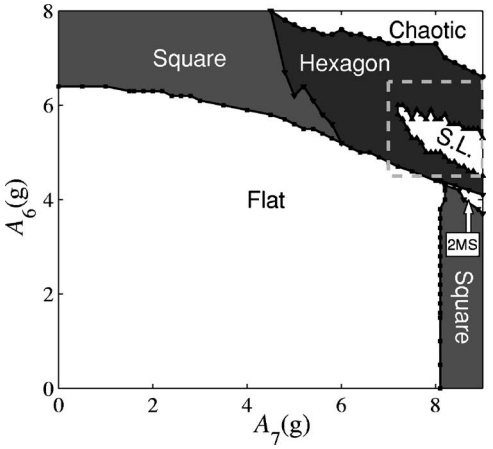

FIG. 2. Unperturbed phase diagram for 6:7 driving with $\omega = 16.5$ Hz and $\phi_7 = 40°$. For hexagons and type-I superlattice patterns (SL), the 6ω driving term is dominant (waves oscillate at 3ω), while for squares and 2MS the 7ω term is dominant. Dashed lines indicate the region where the higher acceleration resolution measurements in Fig. 5 are performed.

TABLE I. Pattern classification.

Pattern	$C_{k_m}(60°)$	$C_{k_m}(30°)$	$C_{k_m}(22°)$	$C_{k_m}(90°)$
Hexagonal	$\geqslant 0.6$	<0.6	<0.6	<0.6
Type-I SL	$\geqslant 0.6$	$\geqslant 0.6$	<0.6	<0.6
12-fold QP	$\geqslant 0.6$	<0.6	$\geqslant 0.6$	<0.6
Square or 2MS	<0.6	<0.6	<0.6	$\geqslant 0.6$
Disordered	<0.6	<0.6	<0.6	<0.6

Patterns of squares are stable when either driving amplitude is dominant, while hexagons, square two-mode superlattice patterns, and 12-fold quasipatterns appear when the amplitudes are comparable. At larger amplitudes, the surface waves are spatially and temporally disordered. To investigate the effect of adding a third frequency, a region of Fig. 1 (as indicated by dashed lines) is examined with higher acceleration resolution ($0.1g$). Figure 3(a) is the phase diagram for 4:5 driving, while Fig. 3(b) shows results for 4:5:2 driving over the same range of A_4 and A_5 but with $\phi_2=32°$ and $A_2=0.8g=0.59A_{2c}$, where $A_{2c}=1.36g$ is the critical acceleration amplitude for single frequency driving at 2ω. Each symbol in the graph represents an experimental data point. Data were also collected in the featureless regions of the figure (below onset), but are not marked by a symbol. Wave onset is typically hysteretic with a magnitude of approximately $0.01g$. Higher resolution measurements of the hysteresis and its dependence on phase will be reported elsewhere [25].

Three main differences exist between the two-frequency and three-frequency phase diagrams. First, the region of stable hexagons becomes much smaller with the addition of the third frequency term. For two-frequency driving, there is a large region of hexagons, but for three-frequency driving, hexagons almost disappear, except for a small area where A_5 is small. Second, the 12-fold quasipattern becomes the primary instability for $A_5 \geqslant 5g$ and most of the region corresponding to hexagons for two-frequency driving converts to 12-fold quasi-patterns with the addition of the finite A_2 term. Third, the transition between ordered patterns and a disordered state occurs at lower driving amplitudes.

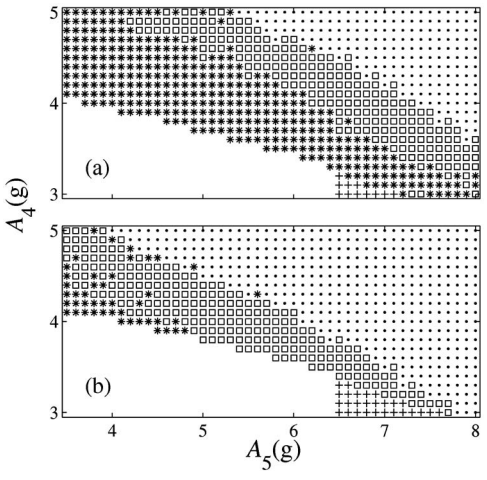

FIG. 3. Phase diagrams for varying A_4 and A_5 with (a) 4:5 and (b) 4:5:2 driving where $\omega/2\pi=20$ Hz and $\phi_5=16°$: hexagons (*), quasipatterns (□), squares and 2MS (+), and disordered (●). Unmarked regions indicate a flat surface state. In (b) the addition of the 2ω term with $A_2=0.8g=0.59A_{2c}$ and $\phi_2=32°$ shifts the quasipattern region to onset, which changes by less than $0.1g$.

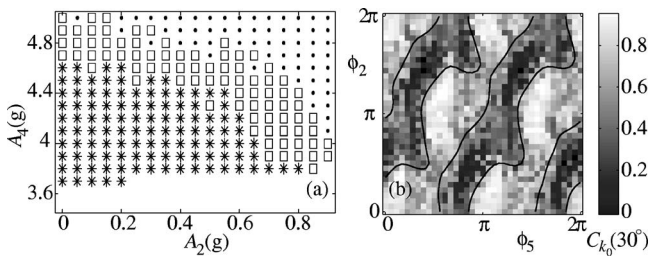

FIG. 4. (a) Phase diagram for 4:5:2 driving with $\{A_5,\phi_2,\phi_5\}=\{5g,32°,16°\}$. The quasipattern region rapidly approaches onset when A_2 exceeds $0.6g=0.44A_{2c}$. Symbols are the same as in Fig. 3. (b) Quasipattern measure $C_{k_m}(30°)$ vs ϕ_2 and ϕ_5 for $\{A_4,A_5,A_2\}=\{3.8g,5.8g,0.8g\}$. The slopes of the large correlation regions (bordered by contours) are roughly 2. In both (a) and (b) $\omega/2\pi=20$ Hz.

Edwards and Fauve reported that the relative phase influences pattern selection for two-frequency driven Faraday waves [12]. Recent experimental work on the stability boundary of hexagonal patterns with two-frequency driven Faraday waves also demonstrates that the phase of the driving function plays an important role in pattern selection [25]. Here, we observe that the relative phases remain important in three-frequency driving. Since only two phases are independent, a two-dimensional phase diagram is used to explore the effect of the phases for fixed driving amplitudes as Fig. 4(b) shows. The amplitudes correspond to a point in the center of the 12-fold quasipattern region in Fig. 3(b). The phases of the driving function clearly affect the stability of the quasipattern with the strongest patterns occurring within roughly linear regions where $\phi_2 \propto 2\phi_5$. Accordingly, the phase diagram is identical for $\phi_5 \rightarrow \phi_5+\pi$. Within the linear regions of stability there are four regions at $\phi_2=0$, $\phi_5=\{0,\pi\}$ and $\phi_2=\pi$, $\phi_5=\{\pi/2,3\pi/2\}$ where the quasipatterns are strongest.

We also observe stabilization and phase dependent effects in type-I superlattice patterns when a third frequency is added (6:7 and 6:7:2 driving) which are similar to those observed in the 12-fold quasipattern experiments. As Fig. 2 shows, squares are again the preferred state when a single amplitude is dominant, and hexagons, square two-mode superlattice patterns, and now type-I super lattice patterns (instead of quasipatterns) are evident in the vicinity of the codimension-2 point with spatiotemporal disorder occurring at larger driving. Unlike quasipatterns, the superlattice state is surrounded by a region of stable hexagons.

The higher acceleration resolution phase diagrams of Fig. 5 show the difference between 6:7 and 6:7:2 driving for the parameter region in Fig. 2 marked by dashed lines. By add-

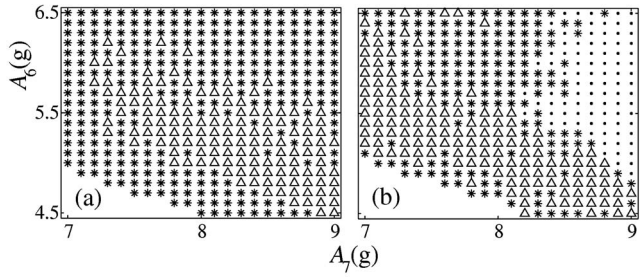

FIG. 5. Phase diagrams for (a) 6:7 and (b) 6:7:2 driving with varying A_6 and A_7 where $\phi_7=40°$ and $\omega/2\pi=16.5$ Hz: superlattice (△), hexagons (*), and disordered (●). In (b) $\phi_2=80°$ and $A_2=0.4g=0.4A_{2c}$.

ing a small amplitude 2ω component with $A_2=0.4g$ (onset occurs at $A_{2c}=1.0g$ for single-frequency driving at 2ω), the phase diagram is significantly altered. The type-I superlattice region moves closer to onset and to lower values of A_7. However, unlike quasipatterns in 4:5:2 driving, when type-I superlattice patterns in 6:7:2 driving lose stability at higher amplitudes, hexagonal patterns or a disordered state appear depending on the value of A_7. Stabilization is sensitive to the magnitude of A_2 as demonstrated in Fig. 6(a). The type-I superlattice is absent for $A_2=0$, but gradually emerges as A_2 increases above $0.2g$. When $A_2 \gtrsim 0.56g$, the disordered state appears, and pattern onset is also higher. Figure 6(b) shows the effect of varying the driving phases ϕ_2 and ϕ_7 for fixed acceleration amplitudes. As was the case for quasipatterns with 4:5:2 driving, type-I superlattice patterns exist within regions where ϕ_2 is proportional to $2\phi_7$. However, for 6:7:2 driving, these regions are devoid of obvious internal structure.

DISCUSSION AND CONCLUSION

In both 12-fold quasi-patterns and type-I superlattice patterns, there is one primary wavelength in the Faraday wave pattern—the 4ω mode in 4:5:2 driving and the 6ω mode in

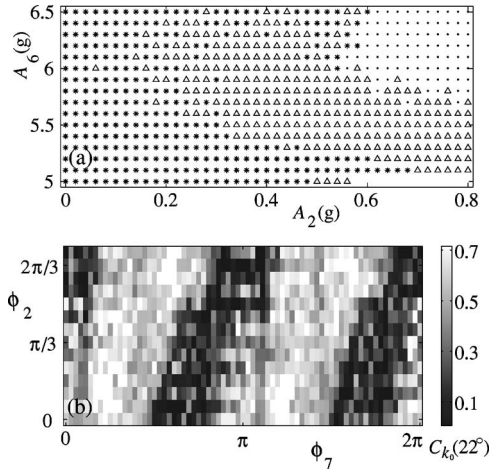

FIG. 6. (a) Phase diagram for varying A_2 and A_6 with $\{A_7,\phi_2,\phi_7\}=\{7.0g,80°,40°\}$. Symbols are the same as in Fig. 5. Super-lattice patterns appear for $A_2 \gtrsim 0.2A_{2c}$. (b) S.L. pattern measure vs. ϕ_2 and ϕ_7 for $\{A_6,A_7,A_2\}=\{5.2g,7.8g,0.6g\}$. In both (a) and (b) $\omega/2\pi=16.5$ Hz.

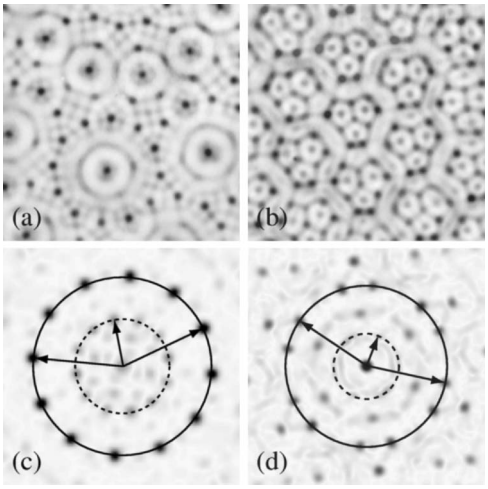

FIG. 7. (a) 12-fold quasipattern with 4:5:2 driving ($\{A_4,A_5,A_2\}=\{3.8,6.0,0.8\}$, $\{\phi_5,\phi_2\}=\{16°,32°\}$, $\omega/2\pi=20$ Hz), and (b) type-I superlattice with 6:7:2 driving ($\{A_6,A_7,A_2\}=\{4.4g,7.4g,0.4g\}$, $\{\phi_7,\phi_2\}=0$, $\omega/2\pi=15$ Hz). Resonant triad construction of patterns illustrated with power spectra from (c) quasipattern image (a), and (d) superlattice image (b). Images (a) and (b) are 5.25×5.25 cm^2. All images have inverted gray scales.

6:7:2 driving. The magnitudes of A_5 and A_2 for quasipatterns and A_7 and A_2 for superlattice patterns are below onset so that their corresponding modes are linearly damped. In a symmetry based analysis, Porter *et al.* [19,22] have shown that the ω linearly damped mode (parametrically excited by the A_2 term) plays an important role in pattern formation. Combined with the wave vectors corresponding to 2ω for quasipatterns or 3ω for superlattices (driven by A_4 or A_6 respectively), resonant triads are formed, as illustrated in Fig. 7. When the resonance conditions are satisfied, $\vec{k}_m+\vec{k}_m=\vec{k}_p$ and the driven damped modes stabilize the corresponding patterns.

As Figs. 3(b) and 5(b) show, 12-fold quasipatterns and type-I superlattice patterns can both become the primary instability when driven with three frequencies, even though the third-frequency amplitude A_2 is only about one-half of its critical value for single-frequency driving at 2ω. Porter *et al.*'s theoretical results indicate that the resonance condition for three-frequency driving $m:n:p$ is affected by a "total" phase Φ defined as [22]

$$\Phi = 2\phi_m - 2\phi_n + \phi_p. \tag{3}$$

The cross-coupling coefficient which enhances the three-wave interaction is maximized when $\sin\Phi \approx \pm 1$. Since the resonance condition requires a linear relation between ϕ_p and $2\phi_n$ (recall that we have set $\phi_m=0$ with no loss of generality), the stable pattern forming regions [see Figs. 4(b) and 6(b)] should form straight bands with slope 2 when plotted as functions of ϕ_n and ϕ_p. Indeed, when $\phi_2 \propto 2\phi_5$, 12-fold quasipatterns are preferred in 4:5:2 driving, and when $\phi_2 \propto 2\phi_7$, type-I superlattice patterns are preferred in 6:7:2 driving. These results provide support for the three-wave resonance Faraday wave pattern selection mechanism via three-frequency forcing proposed by Porter *et al.* [22]. However,

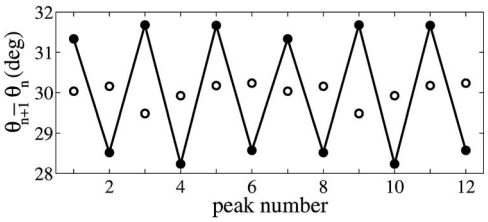

FIG. 8. Angular difference of adjacent peaks in the power spectrum (located at θ_n and θ_{n+1}) on the circle $k=k_4$ illustrating the difference between true 12-fold quasipatterns with 4:5:2 driving (○) and "grid state" 12-fold quasipatterns with 4:5 driving (●). For the grid state quasipattern $\{A_4, A_5\}=\{2.6g, 5.0g\}$, $\phi_5=0$ and $\omega/2\pi=15$ Hz. The true quasipattern data (○) are derived from Fig. 7(c).

the phase diagrams in Figs. 4(b) and 6(b) show that Φ appears shifted by δ from its predicted form, i.e., $\Phi=-2\phi_n+\phi_p+\delta$ with $\delta\approx\pi/2$ and $\delta\approx\pi/3$ for 4:5:2 and 6:7:2 driving respectively. In addition, Fig. 4(b) has structure not predicted by the theory, which may indicate the existence of other interactions sensitive to the relative phases.

Finally, we discuss our results in light of a recent report by Epstein and Fineberg [18] of Faraday wave patterns with 6:7 forcing perturbed by a third driving frequency. In 18 cS shallow layers (0.2 cm and 0.3 cm deep) they find "grid state" patterns for which the 12 constituent wave numbers lie on a hexagonal sublattice. These patterns include a 12-fold quasipatternlike state for which the two underlying hexagonal patterns are rotated by 28° rather than 30° for true 12-fold quasipatterns. In contrast, our experiments reveal true 12-fold quasipatterns with 4:5:2 driving, while grid state 12-fold quasipatterns are seen with 4:5 driving. Figure 8 compares the structure of these two types of patterns by plotting the difference in angle $\theta_{n+1}-\theta_n$ between successive peaks in the power spectra. For 12-fold quasipatterns the difference is always near 30° while for grid state quasipatterns the difference alternates between approximately 28.5° and 31.5° which are close to the values observed by Epstein and Fineberg of 28° and 32° with perturbed 6:7 driving. In our experiments the addition of the third frequency produces a true 12-fold quasipattern while in the experiments of Epstein and Fineberg the third frequency generates grid states. This contrasting behavior could be due to the difference in fluid depth, base frequency, or frequency ratio of the two main modes (i.e., 4:5 vs 6:7). Also, Epstein and Fineberg find that the stability of the type-I superlattice pattern (which they label as a "3:2 grid state") is a function of the total phase Φ with a peak in stability at $\Phi\approx 2\pi/3$, which differs from our finding of maximum stability at $\Phi\approx\pi/6$ for 6:7:2 driving [see Fig. 6(b)]. Additional experiments at intermediate fluid depths could be illuminating.

We have performed high acceleration resolution studies comparing the stability of 12-fold quasipatterns and type-I superlattice patterns driven at two frequencies to the same patterns driven with an additional third frequency at twice the difference of the two original frequencies. In the latter case and with the proper choice of phases and amplitudes, both patterns appear at the linear stability threshold, whereas in the former case, they appear via a secondary instability of a hexagonal pattern. Our experimental results reveal that the third frequency term, when added at the proper frequency and phase and with sufficient magnitude, enhances the stability of both patterns in support of the theory of Silber and co-workers [19–22]. However, there is a difference in the measured and predicted values of the total phase Φ for maximum pattern stability. Because the relative phases affect the resonance mechanism, the phase of the third frequency can be used to switch between different patterns. Adjusting phase, rather than amplitude, may offer a convenient method of pattern control.

ACKNOWLEDGMENTS

We thank Mary Silber, Jeff Porter, and Chad Topaz for helpful discussions and for sharing their theoretical results with us.

[1] M. C. Cross and P. C. Hohenberg, Rev. Mod. Phys. **65**, 851 (1993).
[2] E. Bodenschatz, W. Pesch, and G. Ahlers, Annu. Rev. Fluid Mech. **32**, 709 (2000).
[3] R. C. DiPrima and H. L. Swinney, in *Hydrodynamic Instabilities and the Transition to Turbulence*, 2nd ed., Topics in Applied Physics, Vol. 45 (Springer, Berlin, 1985), pp. 139–180.
[4] H. M. Jaeger, S. R. Nagel, and R. P. Behringer, Rev. Mod. Phys. **68**, 1259 (1996).
[5] P. Grindrod, *The Theory and Applications of Reaction-Diffusion Equations: Patterns and Waves*, 2nd ed., Oxford Applied Mathematics and Computing Science Series (Clarendon Press, Oxford, 1996).
[6] M. Faraday, Philos. Trans. R. Soc. London **121**, 319 (1831).
[7] B. Christiansen, P. Alstrom, and M. T. Levinsen, Phys. Rev. Lett. **68**, 2157 (1992).
[8] A. Kudrolli and J. P. Gollub, Phys. Rev. E **54**, R1052 (1996).
[9] K. Kumar and K. M. S. Bajaj, Phys. Rev. E **52**, R4606 (1995).
[10] D. Binks and W. van de Water, Phys. Rev. Lett. **78**, 4043 (1997).
[11] M. Westra, D. J. Binks, and W. van de Water, J. Fluid Mech. **496**, 1 (2003).
[12] W. S. Edwards and S. Fauve, Phys. Rev. E **47**, R788 (1993).
[13] A. Kudrolli, B. Pier, and J. P. Gollub, Physica D **123**, 99 (1998).
[14] H. Arbell and J. Fineberg, Phys. Rev. Lett. **81**, 4384 (1998).
[15] H. Arbell and J. Fineberg, Phys. Rev. E **65**, 036224 (2002).
[16] H. W. Müller, Phys. Rev. Lett. **71**, 3287 (1993).
[17] T. Epstein and J. Fineberg, Phys. Rev. Lett. **92**, 244502 (2004).
[18] T. Epstein and J. Fineberg Phys. Rev. E (to be published).
[19] J. Porter and M. Silber, Phys. Rev. Lett. **89**, 084501 (2002).
[20] M. Silber and A. C. Skeldon, Phys. Rev. E **59**, 5446 (1999).

[21] C. M. Topaz and M. Silber, Physica D **172**, 1 (2002).
[22] J. Porter, C. M. Topaz, and M. Silber, Phys. Rev. Lett. **93**, 034502 (2004).
[23] Although straightforward to implement, this imaging technique is nonlinear; an image of sinusoidal surface waves contains higher order spatial harmonics. However, they do not affect our results.
[24] E. A. Cerda and E. L. Tirapegui, J. Fluid Mech. **368**, 195 (1998).
[25] Y. Ding and P. Umbanhowar (unpublished).